Imaging formation process for DM profiles

Omar de J. Cabrera-Rosas* and Tonatiuh Matos

Departamento de Física, Centro de Investigación y de Estudios Avanzados del IPN, México Distrito Federal, A.P. 14-740, 07000, México

**E-mail: omar.cabrera@cinvestav.mx*

The imaging formation process in halos for some dark matter profiles is studied. Approaching these models on a small scale, we analyze the images generated on the lens plane by obtaining the analytical surface mass densities $\Sigma(x)$ and their corresponding deflection angles $\alpha(x)$. We identify the presence of Einstein rings, by mapping fringes that represent possible sources (such as other galaxies), placed on the source plane. We approach the simplest case, where lines parallel to the x axis are mapped onto the lens plane, to find out how are the solutions of the $\mathbf{X}$ vector field, which is in this case, the geometrical equivalent to the usual lens mapping.

Keywords: Dark Matter, Gravitational Lensing

1. Introduction

The dynamics of galaxies is a topic of great interest in cosmology. In recent years, this dynamic has been studied with the observation and analysis of the rotation curves of several samples of galaxies. From these observations an acceleration has been measured, and the presence of Dark Matter (DM) is necessary to explain their dynamics.[1,2]

The restrictions belonging to the central surface density of the halo, determine the value of the quantity μ_{DM} which is always a constant, that it seems to be an universal invariant, and there are evidences of this restriction in spiral, dwarf irregulars and ellipticals galaxies to name some types.[3–6] It is important to observe that μ_{DM} is constructed as the product of the characteristic length r_s and the central density value ρ_s of each galaxy, and this is related with the *soliton* region (the core of the galaxy). This is an important zone, because the extra galactic components do not alter this region and the invariant objects present there, are very helpful to understand the complete behavior of the galaxy.[7] In fact, certain models for Scalar Field Dark Matter (SFDM) have predicted that the total mass of these systems is $M_{DM}(300\text{pc}) \sim 10^7 M_\odot$ with a characteristic size $r_s = 300\text{pc}$; that is, the soliton region is perfectly delimited for its analysis, and it is very important for eventual tests that improves the physics interpretation of the data. Therefore, to study the dynamical process for translating this information to the imaging information, this soliton zone must be analyzed, with the corresponding considerations for that region.

In fact, the universal DM profile (the Navarro-Frenk-White profile NFW) has been exhaustively studied, because it fits properly with observational data[8,9];

however, it presents problems on a small scale, which implicates that there must be another models, that explain the core zone.

For the above reasons, a complete optical analysis of this region is in order, using the proper data that comprehends all the physical information encoded in each model, but at the same time with a simplification of the studied equations. Hence, we use the usual gravitational lensing formalism,[10] that contains all the mathematical restrictions to fully understand such optical processes. Hence, we compute the images on the lens plane, as functions of the positions of the sources, the source plane and the redshift, which is encoded into the critical surface mass density Σ_{cr}, that appears in the volumetric density $\rho(r)$ (and thus, into the deflection angle $\alpha(r)$ generated in each physical situation). Therefore, the principal goal for using this approach, is to describe the images generated for recent models of DM, and test which of them behave like the observed data. In this stage of the work, we only study the images generated by objects (fringes) very near to the observation axis, by finding the roots of the equation that represents the mapping in that zone (see Eq. 13 below). This eventually means to translate the optical information obtained from the corresponding images, and link it with the information of the galactic dynamics.

This work is organized as follows. In section 2 we set the basic equations for gravitational lensing, and we obtain the surface mass density and the deflection angle analytically for each profile. In section 3, we establish the $\mathbf{X}$ vector field that describes the ray tracing of the optical process; later we use the method provided in,[11] to study the images that will appear on the lens plane. Finally in section 4, we present the conclusions of this work.

2. Basics equations for gravitational lensing

The configuration for gravitational lensing is as usual[10] , where the source plane, the lens plane and the observer are shown. D_s, D_l and D_{ls} are the distances between observer and source, observer and lens and between lens and source planes, respectively.[10] Now, assume that the DM density profile is given in the form $\rho(x) = \rho_s f(x)$, with ρ_s, r_s and $x = r/r_s$ are the characteristic density, the characteristic radius and the scale radius, respectively; $f(x)$ is any given function of its argument.[2] Hence, it is necessary to find the deflection angle in each case, and because the systems considered here are axially symmetric, the surface mass density and the deflection angle are given by[10]

$$\begin{aligned} \Sigma(\xi) &= \int_{-\infty}^{\infty} \rho(\xi, z) dz, \\ \alpha(x) &= \frac{m(x)}{x}, \end{aligned} \tag{1}$$

Name	$f(x)$	$\Sigma(x)$	$\alpha(x) = m(x)/x$
(1)	(2)	(3)	(4)
Burkert	$\frac{1}{(1+x)(1+x^2)}$	$\beta_B F(x)_B$	$\frac{\sigma_B}{x} g(x)_B$
M-SFDM	$\frac{\sin^2 x}{x^2}$	$\beta_{MsT} F(x)_{MSt}$	$\sigma_{MsT}\left[J_1(2x) + \frac{x^3}{3}\right]$
PI	$\frac{1}{1+x^2}$	$\frac{\beta_{PI}}{\sqrt{1+x^2}}$	$\frac{\sigma_{PI}}{x}(\sqrt{x^2+1}-1)$
Spano	$\frac{1}{(1+x^2)^{3/2}}$	$\frac{\beta_{Sp}}{1+x^2}$	$\frac{\sigma_{Sp}}{x}\ln(1+x^2)$
Wave DM	$\frac{1}{(1+x^2)^8}$	$\frac{\beta_W}{(x^2+1)^{15/2}}$	$\frac{\sigma_W}{x}\left(1 - \frac{1}{(x^2+1)^{13/2}}\right)$
NFW	$\frac{1}{x(1+x)^2}$	$\frac{2\mu_{DM}}{x^2-1} F(x)_{NFW}$	$\frac{4\kappa_s}{x}\left(\ln\frac{x}{2} + \frac{2}{\sqrt{1-x^2}}\operatorname{arctanh}\sqrt{\frac{1-x}{1+x}}\right)$

where the radial coordinate r is related to cylindrical polar coordinates by $r = \sqrt{\xi^2 + z^2}$ and $m(x)$ is the dimensionless mass defined by

$$m(x) = 2\int_0^x \kappa(\xi)\xi d\xi. \tag{2}$$

The shear of the system is

$$\kappa(x) = \Sigma(x)/\Sigma_{cr} \tag{3}$$

and $\Sigma_{cr} = c^2 D_s/(4\pi G D_l D_{ls})$ is the critical surface mass density.

Using Eqs. (1) and (2), it is obtained the above table, by using the Burkert, Multistate-SFDM, PI, Spano, Wave DM and NFW dark matter profiles given in,[2,7] where β and σ are constants that determine the scaling of such core, and they depend on the values of μ_{DM} and κ_s.

For the Burkert profile the $F(x)_B$ function for the surface mass density is given by

$$\begin{aligned} F(x)_B &= \frac{1}{\sqrt{1+x^2}}\left[\frac{\pi}{2} + \operatorname{arctanh}\left(\frac{1}{\sqrt{1+x^2}}\right)\right] \\ &-2\begin{cases} \frac{1}{\sqrt{1-x^2}}\operatorname{arctanh}\sqrt{\frac{1-x}{1+x}} & (x<1), \\ \frac{1}{\sqrt{x^2-1}}\arctan\sqrt{\frac{x-1}{x+1}} & (x>1), \end{cases} \\ &= \frac{1}{\sqrt{2}}\left[\frac{\pi}{2} + \operatorname{arctanh}\left(\frac{1}{\sqrt{2}}\right)\right] - 1 \quad (x=1), \end{aligned} \tag{4}$$

and the $g_B(x)$ function for the deflection angle is

$$g(x)_B = \frac{1}{2}\left[x^2\left(\frac{\pi}{2} + \operatorname{arctanh}\left(\frac{1}{\sqrt{1+x^2}}\right)\right) + \sqrt{1+x^2}\right] + \ln x$$
$$+2\begin{cases} \sqrt{1-x^2}\operatorname{arctanh}\sqrt{\dfrac{1-x}{1+x}} & (x<1), \\ -\sqrt{x^2-1}\arctan\sqrt{\dfrac{x-1}{x+1}} & (x>1), \end{cases} \tag{5}$$
$$= \frac{\pi}{4} + \frac{1}{\sqrt{2}} + \frac{1}{2}\operatorname{arctanh}\frac{1}{\sqrt{2}} \quad (x=1).$$

For the Multi-State profile, the F_{MSt} function for the surface mass density is given by

$$F(x)_{MSt} = J_0(2x) + \frac{\pi}{2}[J_1(2x)\mathbf{H}_0(2x) - J_0(2x)\mathbf{H}_1(2x)], \tag{6}$$

where J_ν are the Bessel functions of the first kind of ν-th order and $\mathbf{H}_\mu$ the Struve functions of μ-th order[12,13]; the F_{NFW} function and the corresponding deflection angle for the NFW profile are given in.[8,9]

3. Imaging formation

Knowing the deflection angle for each case, it is possible to develop the imaging formation process. It will be helpful to express the quantities for describing the optical process, in a cylindrical coordinate basis $\{\hat{\boldsymbol{\varrho}}, \hat{\boldsymbol{\phi}}, \hat{\boldsymbol{z}}\}$. From this information, the imaging mapping is given by the vector field

$$\mathbf{X} = \mathbf{r} + l\hat{\mathbf{R}}_G, \tag{7}$$

where $\hat{\mathbf{R}}_G$ is the gravitational refraction ray given by[11]

$$\hat{\mathbf{R}}_G = \cos\alpha\hat{\boldsymbol{z}} - \sin\alpha\hat{\boldsymbol{\varrho}}, \tag{8}$$

and l is the length from the lens plane $z=0$, to a point on a given deflected light ray.

Using Eq. (7) the deflected light rays are

$$\mathbf{X} = (\varrho - l\sin\alpha)\hat{\boldsymbol{\varrho}} + l\cos\alpha\hat{\boldsymbol{z}}. \tag{9}$$

Consider now a family of one dimensional sources in the region $z>0$, locally described by[11]

$$\mathbf{X} = \mathbf{X}(\eta, n), \tag{10}$$

where n denotes the source and η labels the points on that source. From Eqs. (9) and (10), the images that the observer sees on the lens plane $z=0$, given by all the

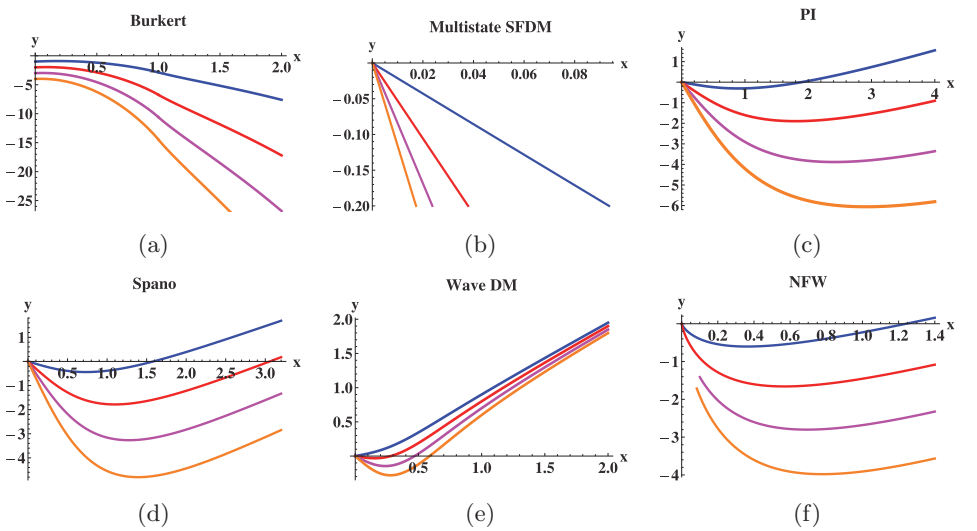

Fig. 1. Plots of the mapping $y = x - z_0\alpha$ for $z_0 = 1, 2, 3, 4$ and $n = 0$. The solutions for $x = 0$ in each profile denote the possible Einstein rings produced in each case. Notice that because in the Burkert and the multistate profiles, the curves does not intersect the horizontal axis, these profiles don't have Einstein rings.

points $(x\cos\phi, x\sin\phi, 0)$, where x and ϕ are solutions to[11]

$$\begin{aligned} X_s(\eta, n) &= [x - Z_s(\eta, n)\alpha(x)]\cos\phi, \\ Y_s(\eta, n) &= [x - Z_s(\eta, n)\alpha(x)]\sin\phi. \end{aligned} \tag{11}$$

Taking the simplest case for line sources that coincide with the x axis, the equations for obtaining the image for each fringe is determined by all the points in the lens plane such that[11]

$$X_s = [x - z_0\alpha(x)]\cos\phi, \tag{12}$$

$$n = [x - z_0\alpha(x)]\sin\phi, \tag{13}$$

with $-L \leq X_s \leq L$.

Now, Eq. (7) encodes the information related with the imaging formation process of the optical system, because describes how is the mapping of points from the lens plane to the source plane; the $\mathbf{X}$ is related with the usual lens mapping.

Because of the axial symmetry of the optical system, the caustic generated by the vector field (7), has a central branch (along the observation axis z). If this branch has contact with the source plane, the observed image is a ring; these are the *Einstein rings*.

In fact, for $n = 0$ (a source aligned exactly with the observation axis), these rings correspond to the roots of Eq. (13), and this is illustrated in Figs. 1. For example,

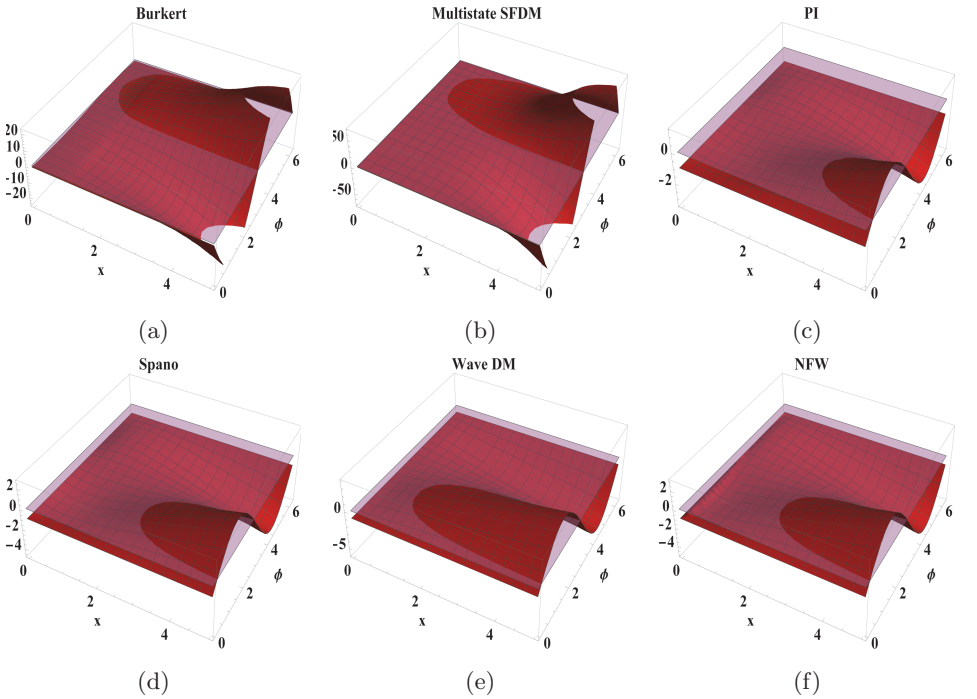

Fig. 2. Schematic of the surfaces representing the solutions of Eq. (13) for each profile on $z_0 = 1$ and $n = 1$. The pink plane intersecting each surface is the $P = 0$ plane. Observe that although the profiles present similar behaviour, the imaging formation process does not begin in the same values of x (neither the values of ϕ are the same).

observe that for the Burkert and Multistate profiles, this function have no roots, hence, they have no presence of Einstein rings for that positions of the source plane.

However, it is important to notice that these rings, are not the only images that could appear in this process. There is another branch of the caustic: a surface of revolution wrapped along the observation axis,[11] that also contributes to the images present on the lens plane, because a change to the source position does not lead to the change of the number of images unless a source moves along a caustic branch,[10] and this situation will appear, if the source and the lens plane are close enough, or in a position where this branch has contact with the source.

In this stage, we are only studying the simplest case, where we are not assuming that the source and the lens are close.

On the other hand, for $n \neq 0$, notice that in general, the deflection angle α is not an invertible function, therefore, it is necessary to find the solutions of Eq. (13) numerically. The above means to analyze Eq. (13) as a family of surfaces labeled by the n index, that are functions of x and ϕ (see Figs. 2).

By analyzing the intersections of these surfaces with the $P = 0$ plane, the image multiplicity according to the deflection angle α (see Fig. 2) can be found. The above

means to be able of identifying the differences on the values of x where the profile begins to generate images, or for the values of ϕ on each quadrant, where the images appear.

An important observation is that it has been shown that the DM central surface density μ_{DM} for all these profiles, is a constant (its values lie in the range $\mu_{DM} = (575 - 648) M_{\odot} \mathrm{pc}^{-2}$)[2,7] and this fact will be very useful for eventual calculations on imaging formation, because this means that the r_s and ρ_s parameters are not independent from each other, and hence by fixing the conditions for one of them, we can establish the correct values for the β and σ parameters.

In fact, because the Navarro-Frenk-White (NFW) profile has been studied in several works,[8,9] it will be important to compare it with the other profiles, and these results must fit with the description of the physical behaviour in DM halos, for later comparing such information with that obtained in the NFW case based on experimental data, but only in the moment where all the profiles can be expressed in a comparable scale.

4. Conclusions

In this work, the analysis for the imaging formation process for dark matter halos has been performed. The goal is to understand if the optical information provided by the lens mapping, gives information about the physical processes that lies in the core of some types of galaxies.

The motivation behind this analysis, was to obtain the analytic equation for the optical mapping from the source plane to the lens plane, and translate directly such information into the images generated on the lens plane.

So far, we have find out that the formation of Einstein rings, depend on the solutions of Eq. (13), that is a projection of the $\mathbf{X}$ vector field (the equivalent of the usual lens mapping) on the lens plane. These calculations are helpful to differentiate the behavior of each profile, and this was carried out by obtaining the deflection angle, encoded in the $\mathbf{X}$ mapping, and later by analyzing the behavior of this function.

This was achieved by plotting the n surfaces that represent the solutions of Eq. (13) to identify the values that correspond to the zones where the imaging formation process begin.

An important observation is that, the ultimate goal for studying such process is to eventually address the problems of the ΛCDM on a small scale, because the NFW profile has problems in this region, and alternative models must be tested there. This means to have at hand an observational tool for testing the possible wave nature of the DM or the species diversity, basing the calculations in the soliton region, because it seems to be that this zone is established by means of an universal invariant μ_{DM} (with the correct values of r_s and ρ_s, that in turn determine our β and σ constants).

Finally, as a future goal based in this work, we consider that we will be able to "draw" the corresponding images mapped from sources (in this case lines) on the lens plane, that represent galaxies or other kind of cosmological objects, by making use of the **X** field. In fact, we already have used this process in the description of a Schwarzschild lens, and the plots allowed us to explicitly identify the positions of the images on the lens plane,[11] that is, by generating images to later compare them with visual data. We believe that the above, can be used as an efficient geometrical way to identify optical configurations, for later interpret the physical data encoded in such images in a nimbly way.

References

1. S. S. McGaugh, F. Lelli and J. M. Schombert, *Radial acceleration relation in rotationally supported galxies*, Phys. Rev. Lett., **117**, 201101 (2016).
2. L. A. Ureña-López, V. H. Robles and T. Matos, *Mass discrepancy-acceleration relation: A universal maximum dark matter acceleration and implications for the ultralight scalar dark matter model*, Phys. Rev. D. **96**, 043005 (2017).
3. M. Spano, M. Marcelin, P. Amram, C. Carignam, B. Epinat and O. Hernández, *GHASP: An H_α kinematic survey of spiral and irregular galaxies — V. Dark matter distribution in 36 nearby spiral galaxies*, MNRAS, 383, 297-316 (2008).
4. F. Donato, G. Gentile, P. Salucci et al,*A constant dark matter halo surface density in galxies* , MNRAS, 397, 1169-1176 (2009).
5. P. Salucci and A. Burkert, *Dark Matter scaling relations*, ApJ **537**, L9 (2000).
6. A. Burkert, *The structure and dark halo core properties of dwarf spheroidal galaxies*, ApJ **808** 158 (2015).
7. L. E. Padilla, J. Solís-López, T. Matos and A. A. Aviléz-López, *Consequences for the Scalar Field Dark Matter Model from the McGaugh Observed-baryon Acceleration Correlation*, The Astrophysical Journal, 909: 162 (16pp), (2021).
8. M. Meneghetti, M. Bartelmann and L. Moscardini, *Cluster cross-sections for strong lensing: analytic and numerical lens models*, Mon. Not. R. Astron. Soc., **340**, 105-114 (2003).
9. G. Golse and J. P. Kneib, *Pseudo elliptical lensing mass model: Application to the NFW mass distribution*, A&A **390**, 821-827 (2002).
10. P. Schneider, C. Kochanek and J. Wambsganss, *Gravitational lensing: strong, weak and micro*, Springer (2006).
11. N. Bretón, O. de J. Cabrera-Rosas, E. Espíndola-Ramos, S. A. Juárez-Reyes, I. Julián-Macías, A. Montiel, P. Ortega-Vidals, E. Román-Hernández, G. Silva-Ortigoza, C. T. Sosa-Sánchez and R. Suárez-Xique, *Towards the Ronchi test for gravitational lenses: the gravitoronchigram*, J. Opt. **19** (2017) 065602 (19pp).
12. I. Gradshteyn and I. Ryzhik, *Table of integrals, series and products*, Academic Press, 7th. Ed. (2007).
13. M. Abramowitz and I. A. Stegun, *Handbook of mathematical functions with formulas, graphs and mathematical tables*, 9th printing (1970).